

Perspective on Afterglows: Numerically Computed Views, Lightcurves and the Analysis of Homogeneous and Structured Jets with Lateral Expansion

Jay D. Salmonson

Lawrence Livermore National Laboratory, Livermore, CA 94551

ABSTRACT

Herein I present numerical calculations of lightcurves of homogeneous and structured afterglows with various lateral expansion rates as seen from any vantage point. Such calculations allow for direct simulation of observable quantities for complex afterglows with arbitrary energy distributions and lateral expansion paradigms. A simple, causal model is suggested for lateral expansion of the jet as it evolves; namely, that the lateral expansion kinetic energy derives from the forward kinetic energy. As such the homogeneous jet model shows that lateral expansion is important at all times in the afterglow evolution and that analytical scaling laws do a poor job at describing the afterglow decay before and after the break. In particular, I find that lateral expansion does not cause a break in the lightcurve as had been predicted. A primary purpose of this paper is to study structured afterglows, which do a good job of reproducing global relationships and correlations in the data and thus suggest the possibility of a universal afterglow model. Simulations of structured jets show a general trend in which jet breaks become more pronounced with increasing viewing angle with respect to the jet axis. In fact, under certain conditions a bump can occur in the lightcurve at the jet break time. I derive scaling relations for this bump and suggest that it may be a source of some bumps in observed lightcurves such as that of GRB 000301C. A couple of lateral expansion models are tested over a range of efficiencies and viewing angles and it is found that lateral expansion can, in some cases, substantially sharpen the jet break. I show flux surface contour maps and simulated images of the afterglows which give insight into how they evolve and determine their lightcurves.

Subject headings: gamma rays: bursts — gamma rays: theory

1. Introduction

It is currently widely believed that gamma-ray bursts (GRBs) derive from narrow (half-opening angle $\theta_{0,GRB} \sim$ few degrees) jets of relativistic ejecta pointing toward the observer. One of the basic motivations for this has been to relieve the energy crisis in GRBs by reducing the necessary total energy from the inferred isotropic equivalent energy (up to several 10^{54} ergs) by a factor $\theta_{0,GRB}^2/2 \sim 10^{-4} - 10^{-6}$ (and thus boosting the total event rate by the reciprocal, $2/\theta_{0,GRB}^2$, to include unseen jets directed away from the observer). If the GRB emission is collimated, it is plausible that the afterglow shock is also colli-

mated into a cone with opening angle θ_0 , generally thought to be larger than $\theta_{0,GRB}$.

A rich area of inquiry is then to predict and look for observable consequences of a narrow jet both in the GRB phase (e.g. Salmonson 2000, 2001) and in the afterglow phase (e.g. Rhoads 1999; Sari et al. 1999). The most fundamental consequences derive from the deceleration of the afterglow as it propagates into the interstellar medium (ISM). The relativistic motion of the emitting shock causes the radiation to be beamed into an angle $1/\Gamma$ in the observer frame. At early times, this relativistic beaming angle is smaller than the physical jet opening angle, $1/\Gamma < \theta_0$, thus the emission appears to be isotropic. Eventually, as the jet de-

celerates, it transitions to $1/\Gamma > \theta_0$ and the finite, non-isotropic extent of the jet becomes apparent to both the observer and to the jet itself. The observer sees a deficit of flux compared to that expected from an isotropic emitter. The jet, now being entirely causally connected, begins to expand sideways. These two effects combine to cause a break in the lightcurve (Rhoads 1999; Sari et al. 1999). Roughly twenty such jet-breaks have been observed (see Frail et al. 2001, and references therein) and these constitute the most direct evidence for beaming to date.

Also, since the later, slower emission is beamed into a wider angle than the earlier emission, we expect to see off-axis optical and radio afterglows where no gamma-ray or X-ray burst was seen (Rhoads 1997; Dalal et al. 2002). To date these so-called ‘‘orphan afterglows’’ have yet to be positively observed.

Thus far the study of this afterglow jet-break has assumed an afterglow pointed directly at the observer with constant, homogeneous, unstructured energy and mass density $\propto H(\theta_0 - \theta)$ across the jet surface, with a hard edge at $\theta = \theta_0$ where $H()$ is the Heaviside step function. As such, from scaling laws, $t_j \propto \theta_0^{8/3}$, the observation of a jet-break time, t_j , gives direct information about the opening angle of the jet. While this model is relatively simple to calculate and is amenable to analytical calculation, it is not necessarily the easiest jet morphology for nature to produce and thus may not accurately represent a physical jet. Firstly, one certainly expects the observers viewing angle, θ_v , of the jet to vary. Furthermore, a homogeneous jet with a hard edge will be unstable to expansion and rarefaction and is thus unlikely to propagate intact and is unlikely to have been formed in the first place. Recent numerical simulations by Zhang et al. (2002) of relativistic jets emerging from stars, within the context of the ‘collapsar’ model, show substantial structure, with the most energetic material along the jet axis and decreasing with larger angles from the axis.

The first semi-analytical calculations of an afterglow jet with structure, i.e. with decreasing energy density and/or Lorentz factor as a function of angle for the jet axis, was done by Rossi et al. (2002) while an analytical treatment was done by Zhang & Mészáros (2002). Not long before, a qualitative discussion of a structured jet model

was put forward by Salmonson & Galama (2002). It was found by Rossi et al. (2002) and Zhang & Mészáros (2002) that a universal structured jet, viewed at different angles, will yield a range of afterglows with jet-break times relating to viewing angle $t_j \propto \theta_v^{8/3}$. By letting the energy per solid angle of the jet decrease with angle from the jet axis, θ , as $\epsilon \propto \theta^{-2}$, they were able to effectively reproduce the observed relation $E \propto t_j^{-1}$ (Frail et al. 2001).

In this paper I present calculations that further refine the work by Rossi et al. (2002) and Zhang & Mészáros (2002). By discretizing the surface of the afterglow, arbitrary functions of energy density, Lorentz factor and lateral Lorentz factor (defined in the fluid frame) can be simulated and lightcurves produced for arbitrary viewing angles θ . In so doing, I corroborate some of the key results of (Rossi et al. 2002; Zhang & Mészáros 2002), i.e. $t_j \propto \theta_v^{8/3}$ and $E_{tot} \propto t_j^{-1}$ if $\epsilon \propto \theta^{-2}$. Also, these more detailed calculations allow for a quantitative discussion of how the lightcurve breaks; in particular I find that a flattening, and even a bump in the lightcurve is possible just prior to the jet-break time. In addition I study lateral expansion and find that some of the general scaling laws that are widely used in afterglow work are incorrect.

2. Numerical Jet Calculations

The calculation presented here begins by discretizing the surface of the afterglow mapped with polar coordinates, (θ, ϕ) , into small elements of solid angle $d\Omega = \cos \psi \sin \theta d\theta d\phi$ where herein we assume the afterglow is spherical, i.e. zero inclination $\psi = 0$, and where $\theta = 0$ corresponds to the jet axis. Each surface element plows into the ISM, sweeping up mass according to its cross-section $dA = R^2 d\Omega$, decelerating, shocking and radiating. The physics of this calculation can be broken up into two parts *i)* the dynamical evolution of each surface element of the afterglow, as dictated by conservation of energy and momentum and *ii)* the radiative mechanism, which I take to be the standard synchrotron shock model (Mészáros & Rees 1997).

To calculate the evolution of the afterglow shock one needs only to invoke conservation of energy and momentum along with an assump-

tion of radiation losses. Herein I assume radiative losses are dynamically insignificant i.e. the evolution is adiabatic. Define the initial bulk Lorentz factor $\Gamma_0 = \mathcal{E}_0/\mathcal{M}_0c^2$ of a surface element of the afterglow, where \mathcal{E}_0 and \mathcal{M}_0 are the initial energy and rest mass per solid angle. Thus following Paczynski & Rhoads (1993) and Rhoads (1999), the energy and radial momentum of a surface element of the afterglow is

$$\begin{aligned}\Gamma_0 + f &= (1 + f)\xi\Gamma \\ \Gamma_0\beta_0 &= (1 + f)\xi\Gamma\beta\end{aligned}\quad (1)$$

where $\xi = (E + M)/M$ is the internal energy of the expanding shell.¹

The mass fraction, f , of accumulated interstellar mass density, $\rho_{ISM} \equiv nm_p$, where m_p is the

¹Eqns (1) are the correct equations for the evolution of jet. It has been noted by several authors (e.g. Huang et al. 2000b) that eqns (1) yield a velocity, $v \propto R^{-3}$, in the non-relativistic limit that is not consistent with the Sedov-Taylor (S-T) blastwave solution, $v \propto R^{-3/2}$, (e.g. Shu 1992). Thus it was assumed that these equations are incorrect for describing afterglow shock dynamics for the entire evolution. There have been alternative formulations of the afterglow shock dynamics. The reason eqns. (1) do not reproduce the S-T solution is because the S-T solution (and the Blandford-McKee (B-M) solution (Blandford & McKee 1976)) is a “blastwave” and as such the fireball does work as it expands and thus radial momentum is not conserved. The S-T solution depends on the assumption of spherical symmetry (the lateral expansion of a fluid element is opposed by expansion of adjacent elements, thus forcing the fluid radially) and thus does not apply to a jet. The jet, having nothing to push on, expands laterally and, thus lacking a radial force, must conserve radial momentum. An afterglow jet is more akin to a bullet fired from a gun than to a spherically expanding blastwave; the jet and the bullet are isolated, momentum conserving bodies decelerating due to their interaction with their surroundings, while the blastwave continues to do work as it expands, by virtue of its sphericity, and thus is not momentum conserving. Thus I argue that eqns. (1) describe the entire evolution of a jet more accurately than do the S-T or B-M solutions in their respective regimes (so long as the jet hasn’t expanded so far as to become spherically symmetric, which I do not find to be the case over the time interval discussed herein). Note that the degeneracy of the energy and momentum equations for $\Gamma \gg 1$ make the behavior of eqns. (1) indistinguishable from the B-M solution in the relativistic regime.

mass of the proton, is

$$\begin{aligned}f &\equiv \frac{\mathcal{M}(R)}{\mathcal{M}_0} = \frac{\Gamma_0c^2}{\mathcal{E}_0} \int_0^R \rho_{ISM} \frac{\Delta\Omega}{\Delta\Omega_0} r^2 dr \\ &= \frac{\Gamma_0m_p c^2}{\mathcal{E}_0\Delta\Omega_0} \Delta N_e = 1.9 \times 10^{-54} \frac{\Gamma_0}{\mathcal{E}_{52}\Delta\Omega_0} \Delta N_e\end{aligned}\quad (2)$$

where the number of electrons swept up into the shock element is

$$\Delta N_e = \int_0^R n_0 \Delta\Omega r^2 dr \quad (3)$$

and the the energy per solid angle is $\mathcal{E}_{52} = \mathcal{E}/(10^{52}/4\pi \text{ ergs})$, and the element solid opening angle is

$$\Delta\Omega = \sin\theta\Delta\phi\Delta\theta \quad (4)$$

where the position of a surface element, θ , will evolve as the shock laterally expands due to internal pressure (Section 3.1). The velocity magnitude is $\beta = |\vec{v}|/c = \sqrt{1 - 1/\Gamma^2}$ and proper time in the fluid frame is

$$t' = \int_0^R \frac{dr}{\Gamma\beta c} \quad (5)$$

Eqns. (1) can be solved for the Lorentz factor

$$\Gamma = \frac{\Gamma_0 + f}{\sqrt{1 + 2\Gamma_0 f + f^2}} \quad (6)$$

So by specifying \mathcal{E}_0 and Γ_0 and a prescription for lateral expansion v_\perp (Section 3.1), the entire evolution of the afterglow as a function of R is determined.

In order to calculate the observed flux, F_ν , at a given frequency, ν , note that the intensity transforms as $I = I'\delta^3$ where the Doppler factor is

$$\delta = [\Gamma(1 - \vec{\beta} \cdot \hat{n})]^{-1} \quad (7)$$

where $\vec{\beta} = \vec{v}/c$ and \hat{n} is the unit vector pointing toward the observer. Following Rossi et al. (2002), here I focus on the power-law branch of the spectrum between the peak, ν_m , and cooling, ν_c , frequencies. As such, the proper intensity at the proper peak frequency, ν'_m , is

$$I'_{\nu'_m} = \frac{P'_{\nu'_m} \Delta N_e}{4\pi R^2 \Delta\Omega} \quad (8)$$

where the shock element has surface area, $R^2\Delta\Omega$, and the proper power per electron radiated at, ν'_m , is (Wijers & Galama 1999)

$$P'_{\nu'_m} = 5.4 \times 10^{-24} \left(\frac{\phi_p}{0.59} \right) n_0^{1/2} \epsilon_{B,-2}^{1/2} \quad (9)$$

$$\times \Gamma \beta^2 \text{ ergs s}^{-1} \text{ Hz}^{-1} \text{ electron}^{-1}. \quad (10)$$

where the factor β^2 has been included here to make this equation valid in the non-relativistic limit (Rybicki & Lightman 1975). The observed intensity at a frequency, ν , is

$$I_\nu = I'_{\nu'_m} \left(\frac{\nu}{\nu'_m} \right)^{-\alpha} \delta^3 \quad (11)$$

and integrating over the population of radiating electrons, the flux will go like

$$F_\nu = \int \frac{P'_{\nu'_m} \Delta A}{4\pi R^2 \Delta\Omega} \left(\frac{\nu}{\nu'_m} \right)^{-\alpha} \delta^3 \frac{(1+z)}{D_L^2} \Delta N_e \quad (12)$$

where D_L is the luminosity distance. The surface area of an afterglow element as seen by the observer, ΔA , is calculated self consistently in the code by projecting the elements onto a surface perpendicular to the observer line of sight. The minimum electron frequency is

$$\nu'_m = 3.5 \times 10^9 \left(\frac{x_p}{0.64} \right) \epsilon_{e,-1}^2 n_0^{1/2} \Gamma^3 \text{ Hz} \quad (13)$$

and $\nu' = \nu/\delta$ where we take $\nu = 4.4 \times 10^{14}$ Hz for the R-band. So

$$\left(\frac{\nu}{\nu'_m} \right)^{-\alpha} = \left[7.96 \times 10^{-6} \left(\frac{x_p}{0.64} \right) \epsilon_{e,-1}^2 n_0^{1/2} \Gamma^3 \delta \right]^\alpha \quad (14)$$

and thus eqn. (11) scales like $I_\nu \propto \Gamma^{3\alpha+1} \delta^{\alpha+3} R \nu^{-\alpha} \propto \Gamma^{3\alpha+2} \delta^{\alpha+4} t \nu^\alpha$, where $t \propto R/\Gamma/\delta$, thus demonstrating the explicit scalings and consistency with Rossi et al. (2002). For $\alpha = 1/2$ the observed flux is

$$F_\nu = 6.4 \times 10^{-57} \left(\frac{\phi_p}{0.59} \right) \left(\frac{x_p}{0.64} \right)^{1/2} \epsilon_{e,-1} n_0 \epsilon_{B,-2}^{3/4} \quad (15)$$

$$\times \frac{2}{1+z} \frac{D_L^2(1)}{D_L^2(z)} \int \Gamma^{5/2} \delta^{7/2} \beta^2 \frac{\Delta A}{R^2 \Delta\Omega} \Delta N_e \text{ mJy}$$

where a cosmology, $(\Omega_b, \Lambda) = (0.3, 0.7)$, was used with $H_0 = 65 \text{ km s}^{-1} \text{ Mpc}^{-1}$ to give $D_L(1) =$

2.2×10^{28} cm. It is important to note that by explicitly evolving Γ (eqn. 6) and F_ν (eqn. 15) in terms of the number of swept up electrons, $N_e \propto$ volume (eqn. 3), this formulation consistently accomodates sideways expansion of the jet (Section 3.1). Finally, the flux lightcurve as a function of observer time, t_{obs} , is calculated by

$$t_{\text{obs}} = (1+z) \int_0^R (1 - \vec{\beta} \cdot \hat{n}) \frac{dr}{\beta c} \quad (16)$$

To better compare physical timescales, the redshift dependence is removed from the times plotted in this paper; $t \equiv t_{\text{obs}}/(1+z)$. Thus we have caste the calculation of the afterglow lightcurve into the state variables of the problem: $R, \Omega, \Gamma, \delta$.

A calculation proceeds as follows. An initial afterglow is specified by $\mathcal{E}(\theta, \phi)$ and $\Gamma_0(\theta, \phi)$ and a lateral expansion prescription and is allowed to plow into the ISM by incrementing the radius by $\Delta R/R \sim$ a few percent. The intensity, eqn. (11) and observer time, eqn. (16) are saved at each surface element. Thus a lattice of (I_ν, t) pairs are evaluated in (θ, ϕ, R) space. Intensity is then interpolated on dataslices of constant observer time t . Finally, the total flux, F_ν , at each observation is derived from eqn. (15) where surface areas, dA , are calculated from a projection of the positions of the observed intensities onto the observer plane of view.

3. Review of Homogeneous Jet Model

It is worthwhile to begin this discussion with a brief review of the homogeneous jet model, which is amenable to analytical calculations and thus allows for comparison and validation of numerical results with known results. The apparent surface area of the afterglow goes like $dA \approx (R \theta_A)^2$ where θ_A is the angular size of the effective viewable aperture onto the afterglow surface

$$\theta_A \approx \begin{cases} 1/\Gamma & \theta_v + 1/\Gamma \ll \theta_0 \\ & \text{(relativistic beaming dominated)} \\ \theta_0 & \theta_v + 1/\Gamma \gg \theta_0 \\ & \text{(physical jet extent dominated)} \end{cases}. \quad (17)$$

Also, one can divide the Doppler factor (eqn. 7) into asymptotic limits

$$\delta \approx 2 \begin{cases} \Gamma & \theta_v \ll 1/\Gamma + \theta_0 \\ 1/(\Gamma\theta_v^2) & \theta_v \gg 1/\Gamma + \theta_0 \end{cases} . \quad (18)$$

Using eqn. (15) the flux at a given frequency is

$$F_\nu \sim \Gamma^{1+3\alpha} \delta^{\alpha+3} R^3 \theta_A^2 \quad (19)$$

and from eqn. (16) the observer time goes like

$$t \approx \frac{R}{\Gamma\delta c} . \quad (20)$$

Before the afterglow shock has reached its deceleration radius, R_d , it coasts freely, $\Gamma \approx \Gamma_0$, and so $\delta \approx \text{const.}$, thus $F_\nu \sim R^3 \sim t^3$, where $t \sim R$. After the shock passes the deceleration radius, i.e. $R > R_d$, the radius and Lorentz factor are related by $R \propto \Gamma^{-2/3}$ (eqns. 2,6). In this regime there exist asymptotic power-law slopes for $F(t)$ only in the simple cases where one of the three angular scales, $\theta_0, \theta_v, 1/\Gamma$, dominates over the other two. These three cases are summarized in Table 1 and can be seen in Fig. 1.

One characteristic timescale of the afterglow model is the deceleration time

$$t_d = \frac{R_d}{\Gamma\delta c} \approx 0.2 (E_{52}/n)^{1/3} \Gamma_{0,1000}^{-8/3} (1 + \Gamma_0^2 \theta_v^2) \text{ s} \quad (21)$$

where I define $R_d = (3E_0/4\pi\Gamma_0^2\rho_{ISM}c^2)^{1/3}$ as the radius at which $f = 1/\Gamma_0$ (eqn. 2). For jets viewed well off axis, $\theta_v \gg 1/\Gamma, \theta_0$, the flux (eqn. 19) varies like $F_d \propto \delta^{7/2}$. Since $t \propto 1/\delta$, then $F_d \propto t^{-7/2}$.

Table 1: The three asymptotic limits where one of the three angular scales, $\theta_0, \theta_v, 1/\Gamma$, dominates the other two. Asymptotic expressions for θ_A and δ are given by eqns. 17 and 18 respectively. In the last column, the expression in parenthesis is for the spectral slope $\alpha = 1/2$ (eqn. 11).

limit	θ_A	δ	Flux ($\alpha = 1/2$)
$\theta_0 \gg \theta_v, 1/\Gamma$	$1/\Gamma$	2Γ	$t^{-3\alpha/2} (t^{-3/4})$
$1/\Gamma \gg \theta_v, \theta_0$	θ_0	2Γ	$t^{-3(2\alpha+1)/4} (t^{-3/2})$
$\theta_v \gg \theta_0, 1/\Gamma$	θ_0	$2/(\Gamma\theta_v^2)$	$t^{3(2-\alpha)} (t^{9/2})$

Another key timescale is the jet-break time, t_j , which occurs when the shock has decelerated to a Lorentz factor $\Gamma \sim 1/\theta_0$

$$t_j = \frac{5}{4} (\Gamma_0 \theta_0)^{8/3} t_d \approx 8.5 (E_{52}/n)^{1/3} \theta_{0,1}^{8/3} \text{ min} \quad (22)$$

where $\theta_{0,1} = \theta_0/1^\circ$. The factor 5/4 derives from eqn. (16) and the fact that the jet-break time occurs when $1/\Gamma \sim \theta_0$ is observed at the *edge* of the jet rather than at the center. This is a factor of 5/2 greater than estimates derived at the jet center (e.g. Sari et al. 1999). For $\theta_v > \theta_0$ the jet break at time t_j is largely washed out, thus a more pertinent timescale in this regime is that at which the flux is a maximum. This occurs roughly when $\theta_v \sim 1/\Gamma \gg \theta_0$, where $\delta \approx 2\Gamma/(1 + \theta_v^2\Gamma^2) \sim \Gamma$ so $F_{\text{max}} \sim \Gamma^4 \sim t^{-3/2}$, where $t \sim \Gamma^{-8/3}$.

The final phase of the afterglow is when the shock motion becomes non-relativistic, $\beta \ll 1$. This regime is beyond the purpose of this paper, however it is necessary to analytically describe the non-relativistic lightcurve behavior of the present model so to understand the asymptotic behavior of the simulations. For $\beta \ll 1$ eqns. (1) yield $\beta \propto R^{-3}$, eqn. (15) goes like $F_\nu \propto R^3 \beta^2$, and eqn. (16) becomes $t \propto R/\beta$. Thus the non-relativistic lightcurve of the present model is $F_{\nu, \text{non-rel.}} \propto t^{-3/4}$. Notice that this is independent of the spectral slope. This non-relativistic model is likely incomplete; for instance Dai & Gou (2001) suggest modifying the shock amplification of the shock-frame magnetic field from $B' \propto \gamma$ to $B' \propto \sqrt{\gamma(\gamma-1)}$. Such modifications can produce substantially different behavior of the afterglow lightcurve, including a break at the relativistic/nonrelativistic transition (Huang et al. 2000a). Since our understanding of such field generation is still incomplete (for example Rossi & Rees 2002), here I choose not to make any such modifications. Let it suffice to understand that all post-break lightcurves modeled in this paper will asymptotically approach $F_\nu \propto t^{-3/4}$ as they approach the non-relativistic regime (for example, see late times of the bottom plot of figs. 4, 5, 6, 7).

In order to validate the results presented here, I compared with existing solutions. Comparing these homogeneous afterglow solutions with those of Granot et al. (1999), I find very good agreement when one accounts for three parameter differences. As mentioned above, eqn. (11) is valid

for observed frequencies above the synchrotron frequency, $\nu > \nu_m$. This simplification is necessary to remove unwanted spectral breaks when attempting to study the cause and quality of dynamical jet breaks. This limit corresponds to the case when parameter $\phi \gg 1$ in Granot et al. (1999). Secondly, Granot et al. (1999) take the velocity of the emitting electrons behind the shock to be $\Gamma/\sqrt{2}$, where I have assumed it to be Γ . I have tested both choices (the former can be implemented by effectively replacing $\Gamma \rightarrow \Gamma/\sqrt{2}$ in eqn. (15)) and find a quantitative difference in the flux surface, but the difference is minimal for the integrated flux; so the shape of the lightcurves is not significantly affected by this choice, as can be seen from the results presented in this section. The last difference is the choice of spectral index; herein the value $\alpha = 1/2$ is employed while Granot et al. (1999) use $\alpha = 3/4$. Adopting the values used by Granot et al. (1999), I find very good agreement with their results.

3.1. Lateral Expansion

Thus far the discussion has concerned jets with no lateral (sideways) expansion, $v_{\perp} = 0$. It has been argued that when $c_s t' \gg \theta_0 c t$, i.e. when the Lorentz factor has decreased such that $1/\Gamma > \theta_0$, where $c_s \sim c$ is the sound speed, the shock will begin expanding sideways (Rhoads 1999; Sari et al. 1999). This increasing angular size of the shock, sweeping up an ever larger region of ISM, is supposed to impede the forward propagation and the shock begins to decelerate exponentially with radius. It is argued that this shift from forward expansion to lateral expansion will cause an exponential decay in Lorentz factor as a function of radius, $\Gamma(R) \propto \exp(-R)$ and thus a break in the afterglow lightcurve. Thus one can derive the predicted post-break lightcurve slope by assuming forward expansion essentially ceases, $R \approx$ constant. Also, if the jet is narrow, then the jet opening angle will expand like $\theta \propto t' \propto 1/\Gamma$ (e.g. Rhoads 1999) and since this physical extent of the jet is growing, one has $\theta_A \sim 1/\Gamma$ (eqn. 17). Thus from eqn. (19) the flux goes like $F_{\nu} \sim \Gamma^{4\alpha+2}$ where $\delta \sim \Gamma$ for $\theta_v = 0^\circ$. Also the observer time varies like $t \sim \Gamma^{-2}$ (eqn. 20). Thus $F_{\nu} \sim t^{-(2\alpha+1)} \sim t^{-2}$ for $\alpha = 1/2$.

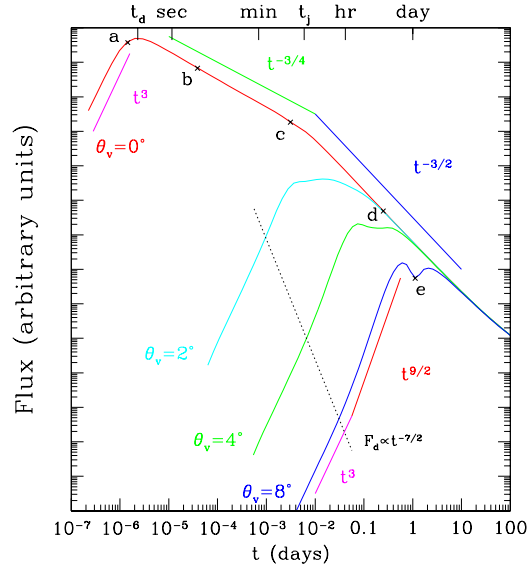


Fig. 1.— Shown are calculated lightcurves for several viewing angles, $\theta_v = 0^\circ, 2^\circ, 4^\circ, 8^\circ$, of an homogeneous afterglow with opening angle $\theta_0 = 1^\circ$ which plows into an ISM with number density $n = 1 \text{ cm}^{-3}$. This afterglow is given an isotropic equivalent energy of 10^{52} ergs and an initial Lorentz factor $\Gamma_0 = 1000$. These curves can be compared with those of Rossi et al. (2002) and thus flux is in arbitrary units and the big tick marks correspond to decades. One can see that the analytical, power-law solutions for each expansion epoch (Table 1) are well reproduced by the numerical calculation. Also, shown along the top axis, for $\theta_v = 0^\circ$, the theoretically predicted deceleration time, $t_d \approx 0.2 \text{ s}$ (eqn. 21) and jet-break time $t_j \approx 8.5 \text{ min}$ (Eqn. 22) correspond well to values calculated numerically. Also shown are asymptotic relationships for the flux at the deceleration time, $F_d \propto t^{-7/2}$ for $\theta_v \gg \theta_0$. It is interesting to note that extrapolating the $\theta_v = 0^\circ$ curves for the free expansion epoch, $F \propto t^3$, and the post-jet-break epoch, $F \propto t^{-3/2}$, as well as the curve $F_{max} \propto t^{-7/2}$, one finds a common point of intersection. This physically corresponds to the lightcurve of a jet of equivalent energy, but with an extremely narrow opening angle $\theta_0 = 1/\Gamma_0$.

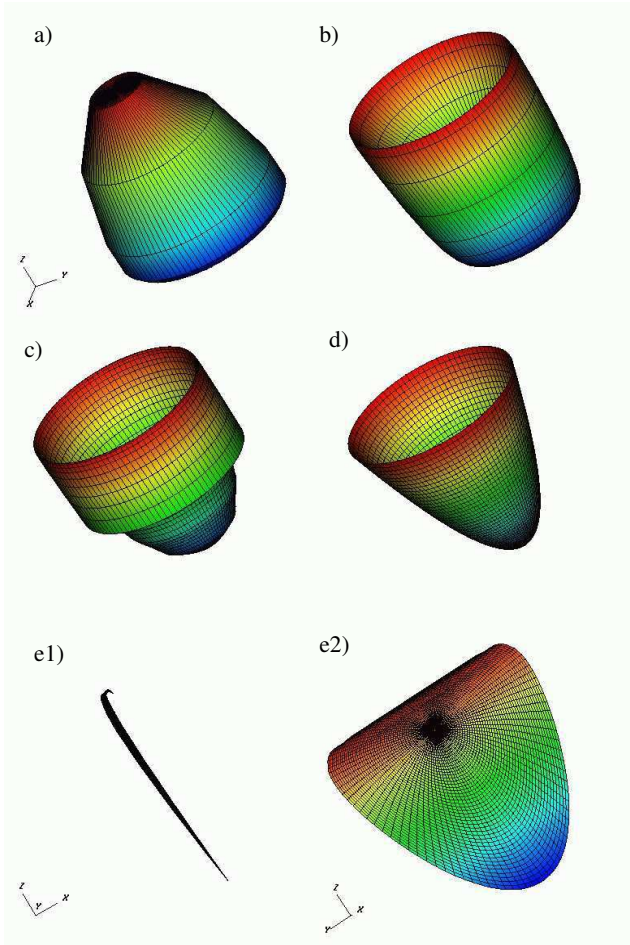


Fig. 2.— Views of the flux contour of the afterglow for various points indicated in Fig. (1). The z-axis is the flux magnitude and the x-y plane is the view plane of the observer, who would be located in the distance to the upper left. Flux (z) and spacial (x and y) axes have been normalized to facilitate viewing. The grid lines demarcate the coordinate surface of the afterglow in (θ, ϕ) at a resolution of $\Delta\theta = 1^\circ/50$, $\Delta\phi = 360^\circ/100$. At a) the shock, which is poorly resolved at this resolution, has not reached the deceleration time (eqn. 21) and thus exhibits a dome-like morphology. After passing the deceleration time (b), the flux becomes concave at the center, as was first described by Granot et al. (1999). This concavity is because the on-axis material is observed to evolve more quickly and thus decelerate and cool faster than off-axis material. In general, larger angles from our viewing axis correspond to earlier times in afterglow evolution and thus higher Lorentz factors, Γ . Physically, the rim of maximum flux around the bowl corresponds to the angle $1/\Gamma$ because material at larger angles having higher Γ and thus tighter beaming, $1/\Gamma$, cannot be seen, and material at smaller angles corresponding to later times has decelerated and thus has reduced flux. The rim thus moves outward as the afterglow evolves. Eventually this rim approaches the physical edge of the jet (c). As the rim passes the edge of the jet, the light curve breaks (d). In (e) we see two views of the afterglow at large viewing angle, $\theta_v = 8^\circ$ at a time when most of the flux is just outside of the rim and thus is basically viewed edge-on by the observer. These calculations do not include the thickness of the shock ($\sim R/\Gamma^2$) and as such one does not expect to observe such a deep notch in a lightcurve at (e) of fig. (1), however, this suggests very high levels of polarization in orphan afterglows.

However, the assumption that the radial expansion in R effectively halts as a result of the lateral expansion of θ_0 is an extreme limit characterized by a narrow opening angle, $\theta_0 \ll 1/\gamma$, and a lateral expansion velocity, assumed constant, that eventually exceeds the decelerating forward velocity. Several workers (Wei & Lu 2000; Moderski et al. 2000; Panaitescu & Mészáros 1999) have shown that in practice the lateral expansion of the jet does not reproduce the scaling discussed above and cannot create a prominent, “sharp” break and instead tends to smooth and broaden the jet-break of eqn. (22). Certainly the approximation of a narrow opening angle does not hold in general and we presently consider the behavior of v_\perp .

The lateral expansion is a result of internal pressure in the shocked medium which, in turn, is the result of the forward motion of the shock into the ISM. Thus I argue that a physically motivated model for lateral expansion is to make the rate of lateral expansion a function of the rate of forward expansion. Thus, one does not expect the lateral expansion velocity to exceed the forward motion of the shock, from which it derives its energy. There are two basic reasons for this. First, as the shock progresses into the ISM, it decelerates, thus the rate of injection of internal energy into the shock from bulk kinetic energy is monotonically decreasing ($\sim \Gamma$). Furthermore the shock is sweeping up interstellar mass at an increasing rate ($\sim R^2$). As was pointed out by Moderski et al. (2000), this mass has no inherent lateral velocity component and thus new mass must be constantly accelerated. This is a significant source of “drag” on the decreasing internal pressure responsible for the expansion. Thus the assumption that lateral expansion is at all times constant is unphysical.

In this section calculations are presented for afterglows with a simple lateral expansion model and it is found that lateral expansion serves primarily to smooth the break if it has any effect at all and, perhaps more importantly, provides very little if any steepening of the post-break light curve.

Each shock element originally moves radially with a Lorentz factor γ . The relativistic jump conditions imply the shocked gas is heated by $\sim \gamma - 1$ and is thus driven to expand laterally via its internal pressure. The actual lateral expansion that results is a complex balance between internal pressure forces of the shocked gas and the “drag” of

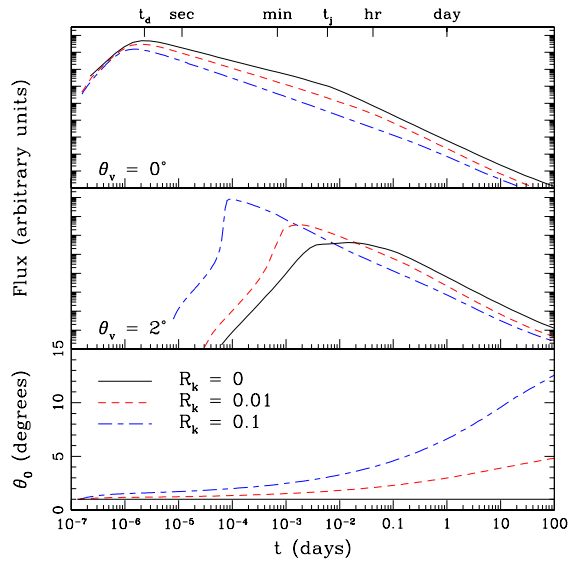


Fig. 3.— Shown are three different lateral expansion rates for an afterglow jet of initial opening angle $\theta_0 = 1^\circ$, initial Lorentz factor $\gamma_0 = 1000$, and isotropic equivalent energy of 10^{52} ergs. These are $R_k = 0$ (no lateral expansion), $R_k = 0.01$, which corresponds to an $\gamma'_\perp = 3.7$, and $R_k = 0.1$, or $\gamma'_\perp = 10.5$. The *top* figure shows the lightcurves as seen on axis, $\theta_v = 0^\circ$, the *middle* plot shows lightcurves viewed at $\theta_v = 2^\circ$. Lateral expansion Doppler boosts the flux into larger angles, θ , from the jet axis and thus on-axis observers see a reduction in flux (top plot) while off-axis observers see a surplus of flux (middle plot). The *bottom* plot show the evolution of the jet opening angle, θ_0 , with observer time. It is important to notice that *none* of these sideways expansion rates shows marked steepening of the lightcurve after the jet break time, t_j , as has been predicted analytically (see Sections 3.1 & 3.2). This is because the growth of θ_0 with time (bottom plot), while rapidly accelerating throughout the evolution, does not become exponential, as analytic arguments would indicate.

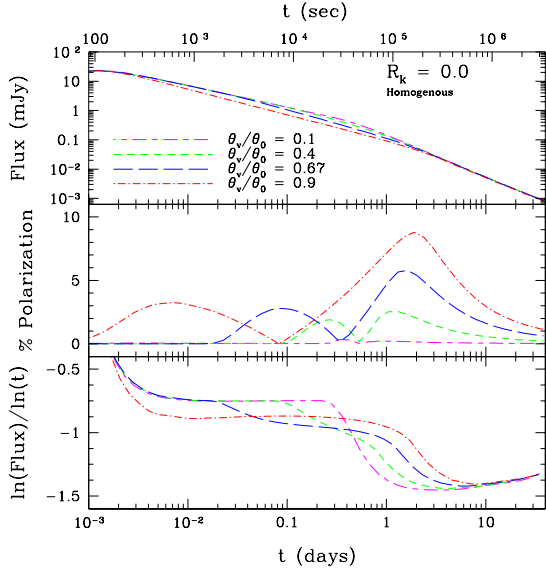


Fig. 4.— R-band lightcurves (top), polarization curves (middle) and power-law index (bottom) for a homogeneous jet with opening angle $\theta_0 = 5^\circ$ and $\mathcal{E} = 10^{52}\text{ergs}/4\pi$, $\Gamma_0 = 100$. The polarization curves closely match those of Ghisellini & Lazzati (1999, Fig. 4). The first peak of the double-peaked polarization curves indicates the “near” edge of the jet coming into view, $1/\Gamma > \theta_0 - \theta_v$, and the second peak corresponds to the “far” edge coming into view, $1/\Gamma > \theta_0 + \theta_v$. Therefore comparison of the three figures shows an initial steepening of the lightcurve for a given viewing angle, θ_v , corresponding to the first polarization peak, and additional steepening occurring at the second peak.

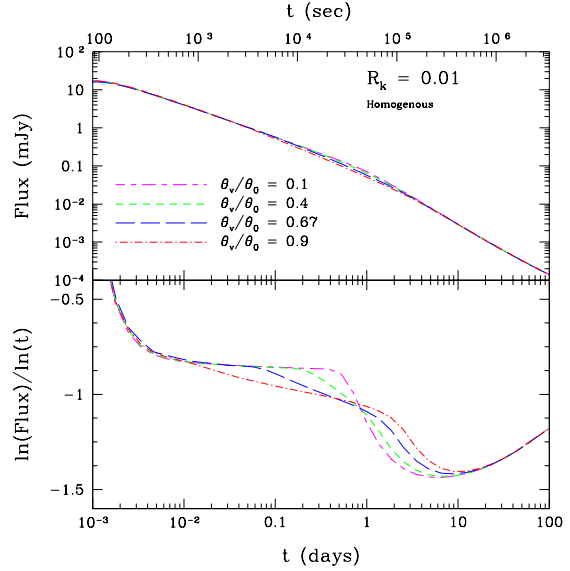


Fig. 5.— The same jet as in Fig. 4, but with sideways expansion (eqn. 23) $R_k = 0.01$, $\gamma'_\perp = 1.6$. The lightcurves are qualitatively similar to those in Fig. 4, with the exception that the lightcurves break later, at around one day, due to the growth of θ_0 prior to that time. The double break is still apparent for larger viewing angles, θ_v , due to the “near” edge of the jet becoming visible before the “far” edge does.

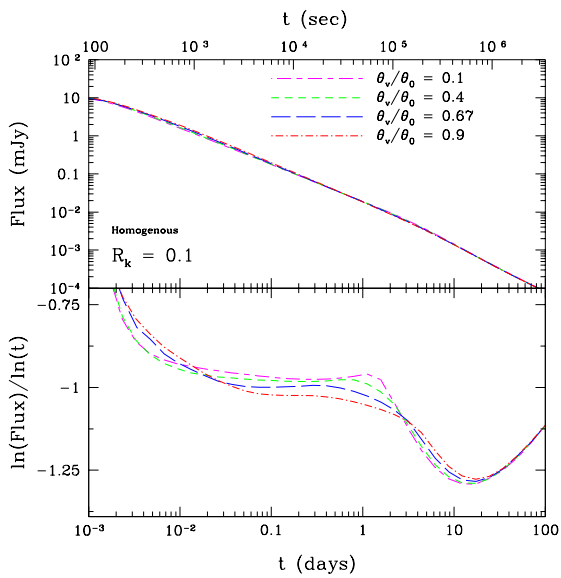


Fig. 6.— The same jet as Figs. 4 & 5, but with a sideways expansion $R_k = 0.1$, $\gamma'_{\perp} = 3.7$. As in Fig. 5, the jet break happens at progressively later times for larger R_k due to the faster rate of growth of the jet opening angle, θ_0 . The double break is no longer readily apparent at larger viewing angles, θ_v . Thus the sideways expansion has “sharpened” the jet edge break.

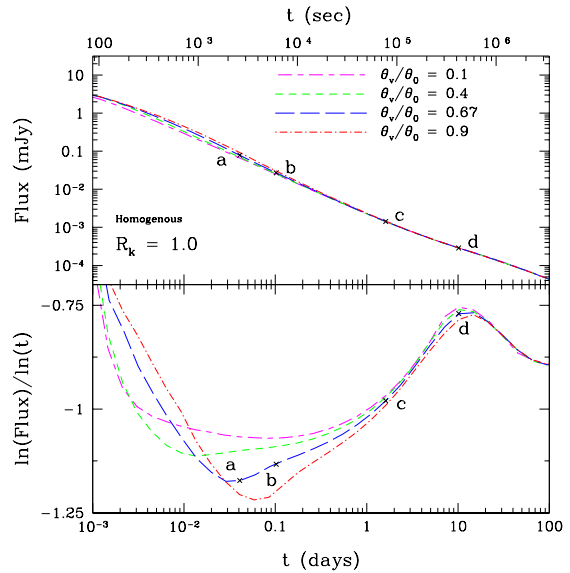


Fig. 7.— The same jet as Figs. 4, 5 & 6, but with sideways expansion $R_k = 1.0$, $\gamma'_{\perp} = 10$. One can see a significant pre-jet-break steepening of the lightcurve circa points a & b as per Section 3.2 and due to Doppler distortions. At later time, point d, the lateral expansion is largely exhausted (Section 3.1) and so the decay slope, $\ln(\text{Flux})/\ln(t) \approx -3/4$, resembles that of the case for no lateral expansion (Fig. 4). Flux contours for selected points on curve $\theta_v/\theta_0 = 0.67$ are shown in Fig. 8.

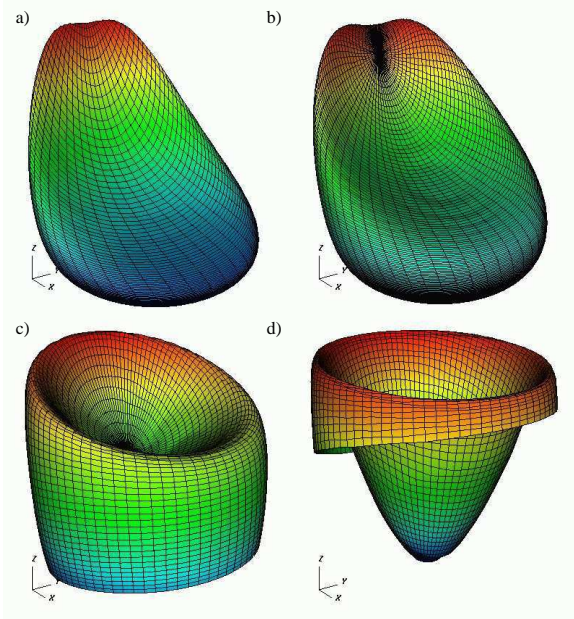


Fig. 8.— Flux contours for selected points of Fig. 7 for $\theta_v/\theta_0 = 0.67$. See Fig. 2 for a description of axes. Plots a) and b) show flux rim (e.g. Fig. 2b) to be heavily skewed and distorted due to the Doppler factor of the sideways expansion; material near the core of the jet is seen to be brighter. In b) the rim expands beyond the pole of the jet. Plot c) shows the rim becoming less distorted as the jet decelerates, but still sloped, and the edge of the jet is visible. Plot d) shows the rim to be very flat and symmetrical as the jet has decelerated substantially thus sideways expansion and resultant aberration has subsided. Grid resolutions are $\Delta\theta = 5^\circ/150$ and $5^\circ/50$ for a) & b) and c) & d) respectively, with $\Delta\phi = 360^\circ/90$.

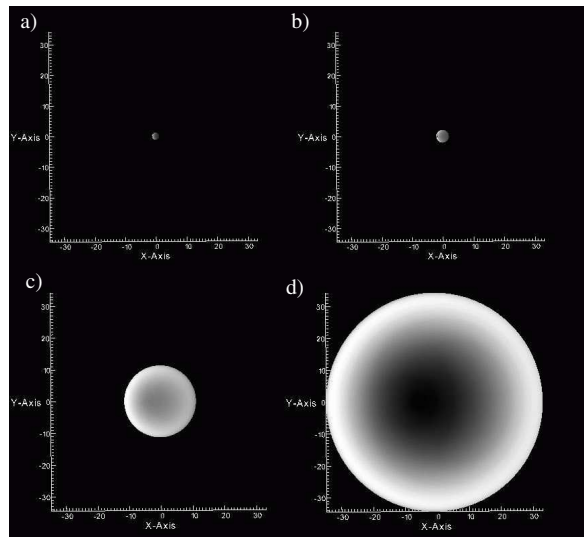


Fig. 9.— What an afterglow might look like. Views of the flux surfaces of the previous Figure 8 along the z-axis. The doppler brightened core is on the left side of the flux surface. Flux magnitude is measured in a normalized color scale; black is zero, white is the maximum. The x and y axes are shown in their true scale and measured in light-days. By comparing with Fig. 7, one can measure the superluminal expansion of the jet.

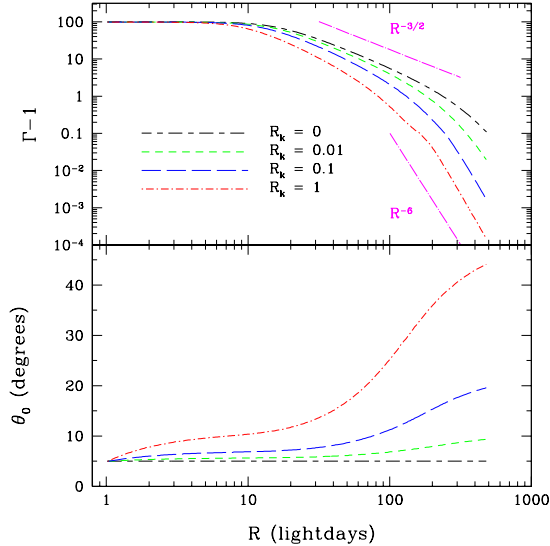


Fig. 10.— For the homogeneous jet model, the evolution of the jet specific kinetic energy, $\Gamma - 1$, and opening angle, θ_0 , are shown for four jet expansion parameters, R_k , (eqn. 23). The kinetic energy (top) does decrease more rapidly with radius, R , for large lateral expansion parameters, but does not become exponential in R as argued by Rhoads (1999). Instead it asymptotically steepens to the nonrelativistic limit, $\Gamma - 1 \propto R^{-6}$. For this reason the sequence of Figs. (4, 5, 6, 7) do not exhibit a progressively more pronounced break due to lateral broadening of the jet. The opening angle (bottom) is seen to expand rapidly once the jet decelerates to roughly $\theta_0 \sim 1/\Gamma$ as expected, but because lateral expansion depends on forward expansion, it slows down to a maximum final opening angle $\theta_{\max} = \theta_0 + \arctan(\sqrt{R_k})$. Since these simulations commence at $R = 1$ lightday (prior to deceleration; $\Gamma \approx \text{constant}$), one can see some early spreading, $\theta_0 \sim \int (v_{\perp}/R) dt \sim \log(R)$. While this particular behavior is an artifact of starting the simulation at $R = 1$ lightday, it does indicate that strong lateral spreading can significantly rearrange the initial jet morphology before it begins to decelerate, thus hinting at the possibility of a universal jet shape independent of initial conditions.

constantly sweeping up and laterally accelerating fresh ISM. This balance depends intimately on the hydromagnetic nature of collisionless shocks and is not well understood as of yet. Here I simply prescribe that the lateral kinetic energy of the shock, in its radially comoving frame, is a constant proportion of the radial kinetic energy. Thus I define this ratio

$$R_k = \frac{\gamma'_{\perp} - 1}{\gamma - 1} \quad (23)$$

which is a parameter measuring the shocks efficiency at converting radial kinetic energy, $\gamma - 1$, into lateral kinetic energy, $\gamma'_{\perp} - 1$, and thus can vary from zero to unity.

Let us define lateral velocity as the velocity of the shock in the radially co-moving frame. This paper assumes axisymmetry of the afterglow so the proper coordinate velocity, 4-velocity and Lorentz factor in this frame are denoted respectively; $v'_{\perp}(\theta)$, $U'_{\perp}(\theta) = v'_{\perp}(\theta)\gamma'_{\perp}(\theta)$, $\gamma'_{\perp} = (1 - v'^2_{\perp}(\theta))^{-1/2}$. Let us assume the shock expands uniformly, i.e. $v_{\perp}(\theta) \propto \theta$ (see Sec. 4.2 for a relaxation of this condition), thus noting that R_k goes like energy, given a ratio, R_{k0} , at the edge of the jet, $\theta = \theta_0$, this ratio at all angles, θ , will be determined by

$$R_k \equiv \left(\frac{\theta}{\theta_0}\right)^2 R_{k0}. \quad (24)$$

It is a convenient fact that since the radial velocity, v , and lateral velocity, v'_{\perp} , are orthogonal in the shock frame, the Lorentz factor of the shock in the lab frame is

$$\Gamma = \gamma\gamma'_{\perp}. \quad (25)$$

where $\gamma = (1 - v^2)^{-1/2}$ and the observer frame lateral expansion velocity is then $v_{\perp} = v'_{\perp}/\gamma$. Thus using eqns. (23,24,25), a given Lorentz factor, Γ , and lateral expansion efficiency, R_k , one can determine γ and γ'_{\perp} . The total Lorentz factor, Γ , is the quantity that is evolved by the dynamical eqn. (6). The angle made by the velocity vector with respect to the *original* radial vector of the shock element, at θ_0 , is

$$\alpha_0 \equiv \arctan\left(\frac{v'_{\perp}}{\gamma v}\right). \quad (26)$$

In other words, we measure the sideways expansion with respect to the original radial vector of the shock element; the shock momentum does not

undergo a torque as θ expands. The angle between the shock element velocity and the radial vector at θ is

$$\alpha = \theta_0 - \theta + \alpha_0 \quad (27)$$

and the shock position, θ , is incremented with radius, R , as

$$\theta(R) = \theta_0 + \int \alpha \frac{dR}{R}. \quad (28)$$

There are many conceivable elaborations of this model. For instance, it is likley that the efficiency of conversion of forward motion to lateral motion is dependent on Lorentz factor and radius, $R_k(\gamma, R)$.

This model implies a maximum asymptotic value for the opening angle θ which is achieved when the shock has decelerated to nonrelativistic velocities, at which eqns. (23,26) imply $\alpha_0 \approx \arctan(\sqrt{R_k})$, and since α will become zero at large radii, then eqn. (28) gives

$$\theta_{\max} = \theta_0 + \arctan(\sqrt{R_k}). \quad (29)$$

Thus, as seen in Figs. 3&10, one does not see exponential growth of the jet opening angle, i.e. $\theta \propto \exp(R)$, and thus the analytically predicted runaway expansions are physically unrealizable.

3.2. Amending the Homogeneous Jet Scaling Laws

An interesting result of these calculations is that the afterglow decay slopes are altered from the theoretical asymptotes both *before* and *after* the jet-break time. In this section I describe why this occurs and give amended analytical asymptotic decay slopes. In Fig. 3 is shown the same homogeneous, narrow, $\theta_0 = 1^\circ$, jet as in Figs. 1 & 2, but now with a range of lateral expansions. A key feature is that, for $\theta_v = 0^\circ$, greater lateral expansion is seen to steepen the lightcurve *prior* to the jet break, while not steepening the lightcurve after the jet break (in fact this slope becomes less steep). This can also be seen in the sequence of Figs. 4, 5, 6, 7 for a more ‘realistic’ jet with $\theta_0 = 5^\circ$. Thus we calculate behavior *opposite* to that predicted by Rhoads (1999); Sari et al. (1999).

To explain this, begin by ignoring Doppler factors, $\delta \propto \Gamma$, thus from eqn. (19) the flux varies

like

$$F_\nu \propto \Gamma^{4(1+\alpha)} R^3 \theta_A^2 \quad (30)$$

and the time (eqn. 20)

$$t \propto \frac{R}{\Gamma^2}. \quad (31)$$

Now parameterizing the Lorentz factor dependence as

$$\Gamma \propto R^{-3\mathcal{A}/2} \quad (32)$$

where \mathcal{A} is unity for the case of no lateral expansion and will be estimated otherwise. These equations with eqn. (17) imply

$$F_\nu \propto \begin{cases} t^{-\frac{1+2\alpha-1/\mathcal{A}}{1+1/(3\mathcal{A})}} & \text{pre-jet-break: } \theta_A \propto 1/\Gamma \\ t^{-\frac{2(1+\alpha)-1/\mathcal{A}}{1+1/(3\mathcal{A})}} & \text{post-jet-break: } \theta_A \propto \theta_0 \end{cases}. \quad (33)$$

In order to estimate the parameter, \mathcal{A} , note from eqn. (2) that

$$f(R) \propto \int (\theta R)^2 dR \quad (34)$$

and from eqns. (28,26) that

$$\theta(R) \approx \theta_0 + \int \frac{dR}{\gamma R}. \quad (35)$$

A crucial point here is that the lab-frame angle between the velocity and radial vectors (eqn. 26), $\alpha_0 \propto 1/\gamma$, and *not* $\alpha_0 \propto 1/\Gamma$. The reason is that maximal sideways expansion occurs when the shock frame lateral expansion energy, γ'_\perp , is roughly the same as the radial expansion energy, γ . From eqn. (25), this implies that total specific energy of the shock, $\Gamma \sim \gamma^2$. So if an expansion angle of $\alpha_0 \sim 1/\Gamma$ is desired, this implies $\gamma'_\perp \sim \Gamma$ and the total specific energy of the shock is $\sim \Gamma^2$ which is energetically untenable. The latter, erroneous choice of α_0 going like $1/\Gamma$ results in the standard exponential decay of Γ with R which was discussed in the first paragraph of Section 3.1. From eqn. (6)

$$\Gamma \approx \sqrt{\frac{\Gamma_0}{2f}} \quad (36)$$

so $1/\gamma \propto 1/\sqrt{\Gamma} \propto f^{1/4}$. Thus one can solve eqns. (34,35) for the asymptotic behaviors. In the limit of no lateral expansion, $\theta(R) \rightarrow \theta_0$, and so eqn. (34) becomes $f \propto R^3$ and thus $\Gamma \propto R^{-3/2}$ so

$\mathcal{A} = 1$ as expected. For the limiting case when lateral expansion dominates, eqn. (35) gives $\theta(R) \rightarrow \int dR/\gamma/R \propto \int f^{1/4}dR/R$ and eqn. (34) becomes $f \propto R^6$ and thus $\Gamma \propto R^{-3}$ so $\mathcal{A} = 2$. Therefore, from eqn. (33), for $\alpha = 1/2$ the pre-break lightcurve is steepened from $F_\nu \propto t^{-3/4}$ for negligible lateral expansion, to $F_\nu \propto t^{-9/7}$ for maximal lateral expansion. This range nicely brackets the pre-break decays of simulated lightcurves over a range of lateral expansion rates as seen in the bottom panel of Figs. (4, 5, 6, 7). It is also worth noting that inspection of Figs. (7, 8) indicates that, not surprisingly, Doppler effects become important for large lateral expansions. Such effects were neglected in the derivation of these scaling laws.

The post-break afterglow decays less steeply than analytical models predicted. This is because, as discussed in Section 3.1, a realistic afterglow jet will expand laterally only in proportion to its forward expansion, thus the lateral expansion rate decreases at late time (see Fig. 10) and the post-break decay curve will asymptotically move toward the limit of no lateral expansion; $\mathcal{A} = 1$.

To summarize, I have implemented a simple model for jet dynamics in which the lateral expansion of the jet is an effect of forward expansion. I argue that this basic cause/effect relationship is a necessary component of any model for jet dynamics. Resulting jet simulations show that lateral expansion *i)* smooths the break in the jet lightcurve, *ii)* steepens the pre-break light curve, but does *not* significantly steepen the post-break slope of the light-curve, *iii)* can significantly alter the shape of a lightcurve. Thus I suggest that the oft-cited scaling laws described at the beginning of this section do not accurately represent the evolution of a laterally expanding jet. To properly diagnose lightcurve slopes and breaks, simulations such as those shown here are necessary. A preliminary conclusion that can be drawn from the simulations shown in this section is that large efficiencies in conversion of forward kinetic energy to lateral kinetic energy, i.e. $R_k \gtrsim 0.1$, are probably not physical, in the context of the homogeneous jet model, because the lightcurves they produce bear little resemblance to observed lightcurves. In this way one can begin to constrain the physics of afterglow shocks with observations.

4. The Structured, Universal Jet

The primary purpose of the numerical framework discussed thus far is to quantitatively study the afterglow lightcurves from structured jets, i.e. with a non-uniform energy or velocity distribution. As suggested by Rossi et al. (2002) and Zhang & Mészáros (2002), an asymptotic decrease in energy per solid angle like $\mathcal{E}(\theta) \propto \theta^{-2}$ can reproduce the observed relation $E \propto t_j^{-1}$ (Frail et al. 2001). Furthermore, allowing $\mathcal{E} \sim \text{constant}$ for angles within a core, $\theta < \theta_c$ provides a natural explanation for the dearth of small angle jets, less than 3° also reported by Frail et al. (2001). As such I define an ansatz energy profile

$$\mathcal{E}(\theta) = \frac{\mathcal{E}_{52}}{1 + (\theta/\theta_c)^2} \frac{10^{52}}{4\pi} \text{ ergs sr}^{-1}. \quad (37)$$

How does one choose an initial $\Gamma_0(\theta)$? based on simulations by Zhang et al. (2002), $\Gamma_0 \sim \text{const.}$ and so this choice will be used for the structured jet runs in this paper. However, it is important to realize, and the following simulations confirm this, that initial Γ_0 only determines the deceleration time of the shock, but subsequent evolution is independent of it. To see this, noting the global energy has dependence $\mathcal{E} \propto \Gamma^2 R^3$ from eqns. (1), then for any radius greater than the deceleration radius, $R > R_d$, the Lorentz factor is determined by $\Gamma \propto \mathcal{E}^{1/2}$, independent of initial Γ_0 .

In Fig. 12 is shown a series of lightcurves from a universal structured jet with isotropic equivalent energy $\mathcal{E} = 10^{53} \text{ ergs}/4\pi$, initial Lorentz factor $\Gamma_0(\theta) = 100$, core angle $\theta_c = 3^\circ$ and $\theta_0 = 30^\circ$. These parameters generally reflect those inferred from burst observations by Panaitescu & Kumar (2002). This figure demonstrates the characteristics of a lightcurve derived from the structured jet described by Rossi et al. (2002).

Using the scaling of eqns. (19, 20) with $\mathcal{E} \propto \gamma^2 R^3$ one finds

$$F_\nu \propto \Gamma^{3\alpha-1} \delta^{\alpha+3} \theta_A^2 \mathcal{E} \quad (38)$$

and

$$t \propto \mathcal{E}^{1/3} \Gamma^{-5/3} \delta^{-1} \quad (39)$$

where the asymptotic limit of θ_A is given in Table 1 and $\delta \approx 2\Gamma/(1 + \theta^2\Gamma^2) \sim \Gamma$ for $\theta \lesssim 1/\Gamma$. Using eqn. (39) and $\mathcal{E} \propto (\theta_c/\theta_v)^{-2}$ for a structured jet, at an early time ($\Gamma \gg 1/\theta_v$) the Lorentz factor

scales with observed angle as $\Gamma \propto \theta_v^{-1/4}$ and so $F_\nu \propto \Gamma^{4\alpha} \mathcal{E} \propto \theta_v^{-(\alpha+2)}$ so the flux at a given time depends on viewing angle like

$$F_{\nu, \text{simultaneous}} \propto \theta_v^{-(\alpha+q)} \propto \theta_v^{-5/2} \quad (40)$$

for $\alpha = 1/2$, and $q = 2$.

There can be seen a gradual flattening, and eventual appearance of a bump, in the lightcurves of Fig. 12 with increasing viewing angle θ_v . This can be understood when one considers that the early phase of the lightcurve, i.e. $\Gamma > 1/\theta_v$, is dominated by emission primarily along the line of sight (los) with energy $\mathcal{E} \propto (\theta_c/\theta_v)^{-2}$, while the flux at the break is dominated by the energetic core moving at angle θ_v with respect to the observer. Here I show that these two components have distinct laws for their breaks, and this difference between these two laws makes each component distinct for large viewing angles, θ_v , thus creating a bump.

The line of sight component can be modeled as a homogeneous jet with opening angle θ_v . As such one expects a break when $\Gamma \sim \delta \sim 1/\theta_A \sim 1/\theta_v$, so $F_{\nu, \text{los}} \propto \Gamma^{4\alpha} \mathcal{E} \propto \theta_v^{-(4\alpha+q)}$. Furthermore $t_{\text{los}} \propto \mathcal{E}^{1/3} \Gamma^{-8/3} \propto \theta_v^2$. So

$$F_{\nu, \text{los}} \propto t_{\text{los}}^{-1/2(4\alpha+q)} \propto t_{\text{los}}^{-2} \quad (41)$$

where $\alpha = 1/2$ and $q = 2$. The jet core component can be modeled as a narrow jet seen far off-axis; $\theta_v \gg \theta_A$ where $\theta_A = \theta_c$. One expects a maximum flux when $\Gamma \sim 1/\theta_v$, thus $F_{\nu, \text{core}} \propto \Gamma^{4\alpha+q} \mathcal{E} \propto \theta_v^{-(4\alpha+q)}$, where $\mathcal{E} = 1$ for the core. It follows that $t_{\text{core}} \propto \mathcal{E}^{1/3} \Gamma^{-8/3} \propto \theta_v^{8/3}$. Thus the core is brightest at

$$F_{\nu, \text{core}} \propto t_{\text{core}}^{-3/8(4\alpha+q)} \propto t_{\text{core}}^{-3/2} \quad (42)$$

for $\alpha = 1/2$ and $q = 2$. This relation traces the jet break in the lightcurve, $F_\nu(t)$, over a range of viewing angles. The different decay laws for eqns. (41, 42) demonstrate why both components of a lightcurve from a structured jet will diverge for large break times. Seen another way:

$$\frac{t_{\text{core}}}{t_{\text{los}}} \propto \theta_v^{2/3}, \quad (43)$$

thus the contribution to the lightcurve from the core happens progressively later than that of the line-of-sight material.

4.0.1. The ‘‘Bump’’

As discussed above, under certain conditions a ‘‘bump’’ can appear in the lightcurve at the jet-break time. This typically happens at large viewing angles and small jet cores. For example, Fig. 11 shows three lightcurves from identical afterglows except for variation in the size of the jet core, θ_c , demonstrating that a narrower core produces a more prominent bump. This bump can be explained by considering how the flux varies as the observer sees an ever-increasing ($\sim 1/\gamma$) angular region of a surface with varying energy density. It can be shown that the observed flux varies like $F \propto \gamma^p \mathcal{E}$ where $p = 2$ for $1/\gamma < \theta_0$ (isotropic) and $p = 4$ otherwise (jet-like). Also, the energy per steradian of the afterglow goes like $\epsilon \propto (\theta_c/\theta)^q$ where in this case $q = 2$. Thus the flux will vary like

$$F(1/\gamma) \propto \left(\frac{1}{\gamma}\right)^{-p} \left(\frac{\theta_c}{\theta}\right) \left(\frac{\theta_c}{\theta - 1/\gamma}\right)^{q-1} \quad (44)$$

so that early in the evolution, when $1/\gamma \ll \theta$, the flux is down by $(\theta_c/\theta)^q$ as expected, but when the beaming angle has expanded to reach the core, i.e. $1/\gamma = \theta - \theta_c$, the flux averaged over the surface will be $\propto (\theta_c/\theta)^{q-1}$. The flux of eqn. (44) decreases as γ decreases until $1/\gamma = p/(p+q-1)\theta$. So the smaller q/p is, the farther out the bump will occur. The condition for *no* bump to be observed is when the jet core becomes visible, i.e. $1/\gamma = \theta - \theta_c$, the flux has not yet begun to increase, thus

$$\theta_c > \frac{q-1}{p+q-1} \theta. \quad (45)$$

So for $p = 2$ and $q = 2$ we have $\theta_c > \theta/3$ and so a bump will be visible if the jet is viewed at angles, θ , much in excess of $3\theta_c$. This analysis is born out in the simulations and gives constraints on the range of allowed viewing angles, θ , with respect to the size of jet core, θ_c , and the steepness of the jet decay structure, q .

There are several examples of bumps in lightcurves including GRB 970228, GRB 970508, GRB 980326 (for a discussion, see Zhang & Mészáros 2002). While in general gamma-ray burst afterglows do not exhibit bumps in their lightcurves just prior to the break, GRB 000301C exhibited a prominent, achromatic bump at the jet-break time which has been interpreted as a gravitational

lensing event (Garnavich et al. 2000) and alternatively as continuous energy injection by a millisecond pulsar (Zhang & Mészáros 2001). In light of the present calculations, it is possible that the bump in the lightcurve of GRB 000301C was due to a simple perspective effect onto a jet with a narrow core or a steep decay curve. This explanation is appealing in that it does not require external mediators (i.e. a lensing body or a pulsar) to create it. If the bump in GRB 000301C and possibly those of other burst lightcurves could be positively attributed to perspective onto a structured afterglow, key information could be determined about the size (i.e. the jet core θ_c) and shape (the decay structure q) of the afterglow.

4.1. Uniform Lateral Expansion

Having constructed a structured jet model, we are interested in the effects of lateral expansion on said model. Since the evolution of the afterglow shock is uncertain, I choose to study two basic paradigms. First, in this section I simply apply uniform expansion to the afterglow as was done for the homogeneous jet in the previous section. Thus expansion is governed by eqn. (24). The second model, discussed in the next section, employs nonuniform expansion, where the hotter core expands faster than the cooler wings of the afterglow.

Examination of the progression of increasing lateral expansions Figs. 12, 13 & 15 shows that lateral expansion suppresses the bump at the jet break time viewed at large θ_v . However, this also makes the breaks at small θ_v less pronounced. This behavior, where the jet break is more pronounced at high viewing angles, θ_v , than at small ones, is quite general. Even a nonuniform expansion paradigm discussed in the next section demonstrates this.

4.2. Nonuniform Lateral Expansion

Uniform expansion of the structured jet is likely oversimplified. A more accurate sideways expansion prescription should encapsulate one's hydrodynamic intuition that a fluid element will be accelerated proportionally to the gradient of its internal energy density. A simple model with this characteristic is

$$R_k(\theta) = R_{k0} \left(1 - \frac{\mathcal{E}(\theta)}{\mathcal{E}_{52}} \right) = R_{k0} \frac{(\theta/\theta_c)^2}{1 + (\theta/\theta_c)^2} \quad (46)$$

using eqn. (37) and where θ_c is not constant, but allowed to laterally expand with the jet by staying assigned to a particular fluid element. Notice that eqn. (46) replicates the uniform expansion of eqn. (24) for small angles, $\theta \ll \theta_c$, but transitions to a constant, rigid-body, expansion for large angles. Figs. 16 & 17 demonstrate that non-uniform expansion can be very effective at creating a very sharp break in the lightcurve.

A key approximation of eqn. (46) is that it assumes a fixed functional form for R_k even as the shock surface evolves. This represents a model in which the proper hydrodynamic timescale, which increases with time, become longer than the deceleration timescale, thus the early time expansion morphology is ‘‘frozen in’’ and predominantly determines the subsequent evolution. Further work is required to determine the hydrodynamical evolution of the afterglow.

5. Discussion

I have implemented a simple model for afterglow jet spreading in which lateral expansion depends upon energy from forward expansion. This model demonstrates that a homogeneous jet does not exhibit a lateral expansion dominated phase, as described by analytical arguments (Rhoads 1999; Sari et al. 1999). In particular, dynamically $\gamma \approx \exp(-R)$, (Fig. 10) and observationally $F_\nu \approx t^{-p}$ after the break, (Figs. 5, 6, 7). The only source of a break in this model is the observation of the physical edge of the jet. As shown in Figs. 5, 6, 7, this break is ‘sharpened’ by lateral expansion in that it becomes less dependent on viewing angle.

Also, I have studied structured jets as seen at various viewing angles and with various sideways expansions. This study confirms the key results of Rossi et al. (2002); Zhang & Mészáros (2002), $t_j \propto \theta_v^{8/3}$ and $E_{iso} \propto t_j^{-1}$. Furthermore, the jet break is seen to be sharp and can exhibit some flattening and even a bump prior to the break at large viewing angles compared to the core size, $\theta_v \gg \theta_c$. It appears to be a general feature of the universal jet model that late time jet breaks (i.e. large θ_v) are more pronounced than early time breaks. That is, if early time breaks are sharp, then late time breaks will tend to have a flattening or a bump (e.g. Fig. 13), but if this bump

is quenched, perhaps by nonuniform spreading of the jet, the early-time breaks become weak or are washed out altogether (e.g. Fig. 17). In general, the sharpness of the structured jet break is determined by the size of the core, $t \propto \theta_c^{8/3}$, and is thus intrinsically sharper than the break in the homogeneous jet model which depends upon the outside edge $t \propto \theta_0^{8/3}$. As such the structured jet can explain sharper breaks than the homogeneous jet model.

Future work with E. Rossi et al. will focus on polarization (e.g. Fig. 4) as a tool to discriminate between the homogeneous and structured jet paradigms. Also, improved understanding of the evolution of the jet, whether it be hydrodynamic or otherwise, will allow for more quantitative expansion models and more predictive simulations.

I wish to convey my sincerest thanks to E. Ramirez-Ruiz, E. Rossi, D. Lazzatti and M. Rees for their kind hospitality at the U. of Cambridge and insightful, enjoyable discussions during the preparation of this document. I also wish to thank T. Galama and R. Sari for stimulating, useful discussions regarding this work. This work was performed under the auspices of the U.S. Department of Energy by University of California Lawrence Livermore National Laboratory under contract W-7405-ENG-48.

REFERENCES

- Blandford R. D., McKee C. F. 1976, *Physics of Fluids*, 19, 1130
- Dai Z. G., Gou L. J. 2001, *ApJ*, 552, 72
- Dalal N., Griest K., Pruet J. 2002, *ApJ*, 564, 209
- Frail D. A. et al. 2001, *ApJ*, 562, L55
- Garnavich P. M., Loeb A., Stanek K. Z. 2000, *ApJ*, 544, L11
- Ghisellini G., Lazzati D. 1999, *MNRAS*, 309, L7
- Granot J., Piran T., Sari R. 1999, *ApJ*, 513, 679
- Huang Y. F., Dai Z. G., Lu T. 2000a, *MNRAS*, 316, 943
- Huang Y. F., Dai Z. G., Lu T. 2000b, *A&A*, 355, L43
- Mészáros P., Rees M. J. 1997, *ApJ*, 476, 232
- Moderski R., Sikora M., Bulik T. 2000, *ApJ*, 529, 151
- Paczynski B., Rhoads J. E. 1993, *ApJ*, 418, L5
- Panaitescu A., Kumar P. 2002, *ApJ*, 571, 779
- Panaitescu A., Mészáros P. 1999, *ApJ*, 526, 707
- Rhoads J. E. 1997, *ApJ*, 487, L1
- Rhoads J. E. 1999, *ApJ*, 525, 737
- Rossi E., Lazzati D., Rees M. J. 2002, *MNRAS*, 332, 945
- Rossi E., Rees M. J. 2002, *MNRAS* in press; *astro-ph/0204406*
- Rybicki J. B., Lightman A. P. 1975, *Radiative Processes in Astrophysics*, USA: John Wiley & Sons, Inc.
- Salmonson J. D., Galama T. J. 2002, *ApJ*, 569, 682
- Salmonson J. D. 2001, *ApJ*, 546, L29
- Salmonson J. D. 2000, *ApJ*, 544, L115
- Sari R., Piran T., Halpern J. P. 1999, *ApJ*, 519, L17
- Shu F. H. 1992, *Physics of Astrophysics*, Vol. 2: Gas dynamics, University Science Books, Mill Valley, CA
- Wei D. M., Lu T. 2000, *ApJ*, 541, 203
- Wijers R. A. M. J., Galama T. J. 1999, *ApJ*, 523, 177
- Zhang B., Mészáros P. 2001, *ApJ*, 552, L35
- Zhang B., Mészáros P. 2002, *ApJ*, 566, 712
- Zhang B., Mészáros P. 2002, *ApJ*, 571, 876
- Zhang W., Woosley S. E., MacFadyen A. I. 2003, *ApJ*, 586, 356

This 2-column preprint was prepared with the AAS L^AT_EX macros v5.0.

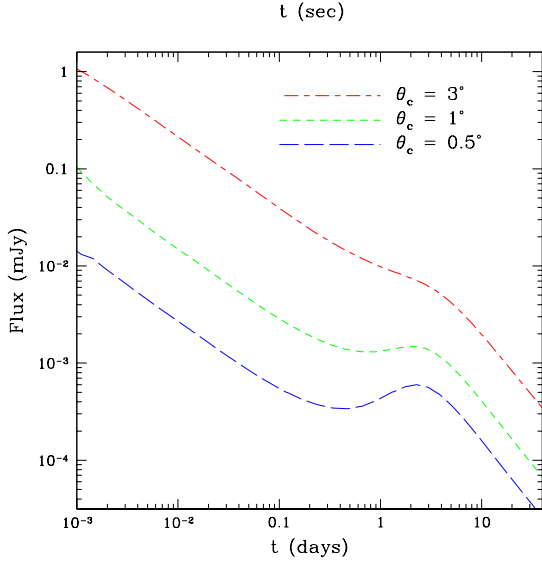


Fig. 11.— The bump in the lightcurves at the jet break time becomes more prominent with smaller cores. These afterglows have $E_{iso} = 10^{52}$ ergs, $\gamma_0 = 100$, $v_{\perp} = 0$, and are seen at $\theta_v = 12^\circ$.

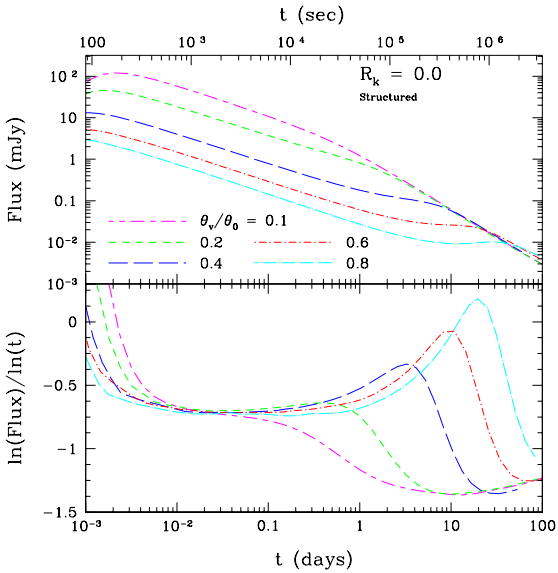


Fig. 12.— Lightcurves for a structured jet with isotropic equivalent energy 10^{53} ergs, $\mathcal{E}_{52} = 10$, using eqn. (37), and initial Lorentz factor $\Gamma_0 = 100$ everywhere. One sees corroboration of the basic thesis of Rossi et al. (2002), with some flattening at larger viewing angles.

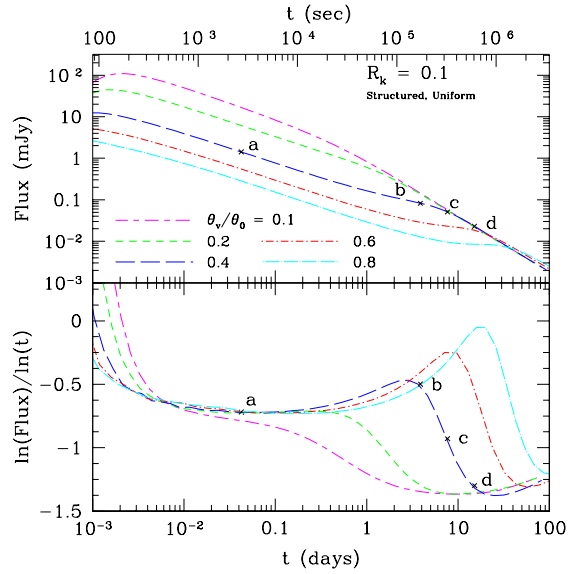


Fig. 13.— Lightcurves for the same structured jet as Fig. 12, but with moderate uniform lateral expansion, $R_k = 0.1$. Notice a slight suppression of the bump at the jet-break time for large θ_v/θ_0 compared to Fig. 12. Fig. 14 shows selected flux contours for $\theta_v = 12^\circ$.

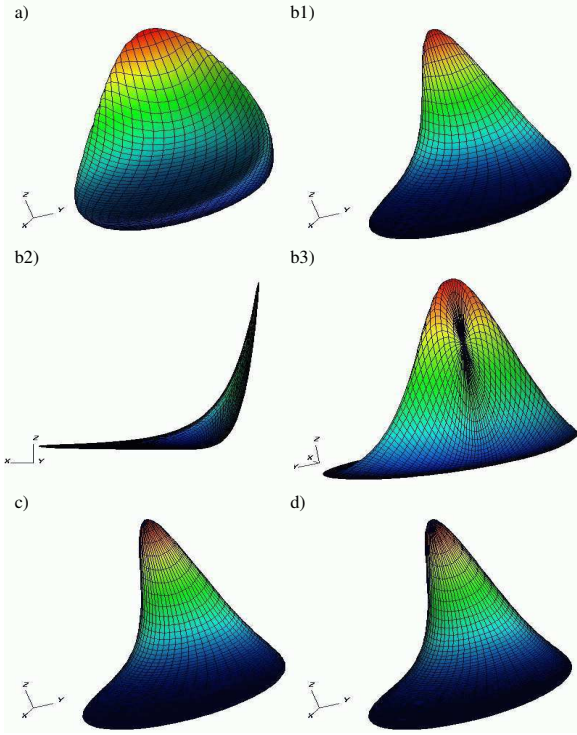


Fig. 14.— Flux contours for selected points of Fig. 13 for $\theta_v = 12^\circ$. At early times, a), the flux surface is distorted from a symmetric bowl (see Fig. 1 b) by both lateral expansion, as in Fig. 8 a), and the intrinsic structure of the jet. Near the jet-break time plots b) show different views of the flux surface. Plot b3) shows the physical pole of the afterglow nearly coincident with the flux peak. This demonstrates the origin of the break in the lightcurve in the structured jet model: the coincidence of the peak flux rim and the actual pole of the jet. As such the edge of the jet does not play a role in the jet break as it does in the homogeneous jets. Plots c) and d) show this coincidence clearly. Grid resolutions are $\Delta\theta = 30^\circ/300$, $\Delta\phi = 360^\circ/360$ for a) and $\Delta\theta = 30^\circ/100$, $\Delta\phi = 360^\circ/60$ for b), c) and d).

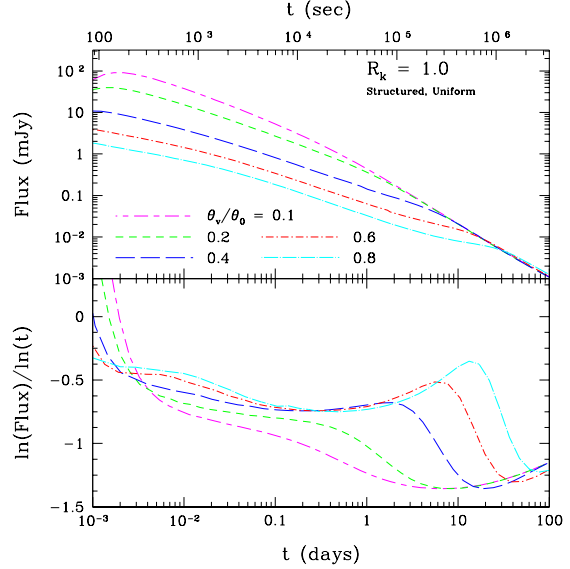


Fig. 15.— Lightcurves for the structured jet of Fig. 12 with large, uniform lateral expansion, $R_k = 1$. Lateral expansion suppresses and smooths the bump in the lightcurve at the jet break time for large viewing angles, θ_v .

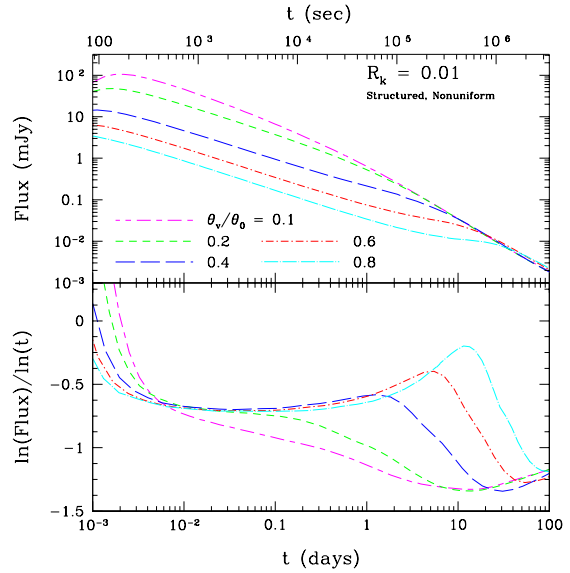


Fig. 16.— Lightcurves for a structured jet with a nonuniform lateral expansion (eqn. 46). Other parameters are the same as in Fig. 12. One can see that even a rather small, $R_k = 0.01$, nonuniform lateral expansion can affect the lightcurves when compared to $R_k = 0$ in Fig. 12.

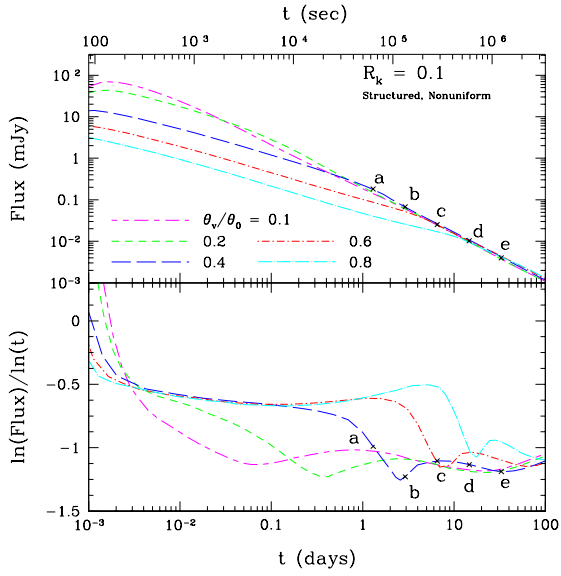


Fig. 17.— The modest nonuniform expansion shown here, $R_k = 0.1$, compared to Figs. 16 & 12 makes a very sharp break with no bump for $\theta_v > 0.2\theta_0$, but washes out the break as seen at smaller viewing angles. Fig. 18 shows selected flux contours for $\theta_v = 12^\circ$.

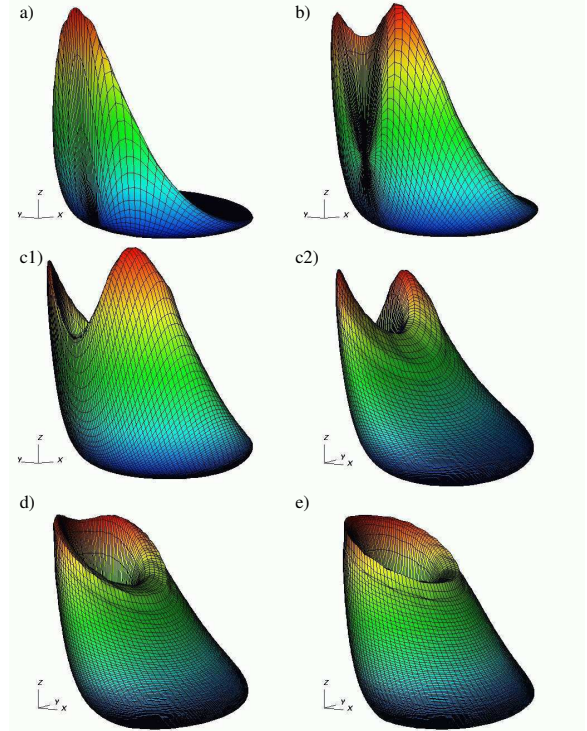


Fig. 18.— Selected flux surfaces for a structured jet with a nonuniform expansion paradigm at $\theta_v = 12^\circ$. Grid resolutions are $\Delta\theta = 30^\circ/100$ and $\Delta\phi = 360^\circ/120$. Prior to the break, a), the morphology is similar to the uniform expansion (Fig. 14). The hot core of the jet expands and decelerates more rapidly than the wings. Thus a crater appears as the core comes into view (b - e). This sharp flux deficit makes a sharp jet-break (Fig. 17).